Journal of Molecular Liquids 245 (2017) 109–114

Contents lists available at ScienceDirect

Journal of Molecular Liquids

journal homepage: www.elsevier.com/locate/molliq

Complete virus capsid at all-atom resolution: Simulations using molecular dynamics and hybrid molecular dynamics/hydrodynamics methods reveal semipermeable membrane function

Elvira Tarasova [a], Ivan Korotkin [b,d], Vladimir Farafonov [c], Sergey Karabasov [d], Dmitry Nerukh [e,*]

[a] Immanuel Kant Baltic Federal University, A. Nevskogo str. 14, Kaliningrad 236041, Russian Federation
[b] Nuclear Safety Institute of Russian Academy of Sciences, Bolshaya Tulskaya 52, Moscow 115191, Russian Federation
[c] Department of Physical Chemistry, V.N. Karazin Kharkiv National University, Svobody Square 4, Kharkiv 61022, Ukraine
[d] School of Engineering and Materials Science, Queen Mary University of London, Mile End, London E1 4NS, UK
[e] Systems Analytics Research Institute, Aston University, Birmingham B4 7ET, UK

ARTICLE INFO

Article history:
Received 15 March 2017
Received in revised form 26 June 2017
Accepted 28 June 2017
Available online 29 June 2017

Keywords:
All-atom simulation of viruses
Hybrid molecular dynamics/hydrodynamics
Multiscale simulations

ABSTRACT

Simulations of complete virus capsid at atomistic details have been performed using standard molecular dynamics as well as original hybrid molecular dynamics/hydrodynamics methodologies. The results show that the capsid is stable in water solution at room temperature and ions composition similar to physiological conditions. Detailed analysis of the flow of water molecules and ions through the capsid's wall is performed. It demonstrates that ions do not cross the capsid shell, while water exhibits substantial flows in both directions. This behaviour can be classified as a semipermeable membrane and may play a role in mechanical properties of the virus particle.

1. Introduction

Modern experimental techniques have reached resolution high enough to measure the structure of entire viruses at atomistic level [1–5]. This provides a unique opportunity to model them using classical molecular dynamics (MD) approaches producing very important biomolecular information on the details of virus functioning, which, in turn, can be used for designing methods of manipulating and deactivating viruses.

Unfortunately, the experiments are usually restricted to detect only static and symmetric parts of the structure, while the dynamics of viral structures is important for representing specific interactions between viral parts, the solution, and cell membrane. Also, the experimental data is performed at low temperature and does not reflect the influence of physiological solution on the sample. However, it is known that water is important for the dynamics of the protein when molecules of water guide the protein adjustment and movements [6].

The solution of this problem is provided by theoretic and computational modelling that have been developed dramatically during recent years [5–12]. Fortunately, the development of new approaches coincide with the development of new powerful computer clusters, including specialised ones [13,14], that allow to perform very large scale simulations with millions of atoms for significant time. Therefore, now there is a great opportunity to investigate atomistic and molecular properties of the viral particles and suggest directions of further experimental developments. This approach will help us to understand the logic of some viral processes that are hidden in the dynamics, interactions with the solution that take place at short times. This complementary experimental and theoretical approach will help us to save time and resources for experimental research and suggest ways of developing effective treatment of virus infections.

In this paper we present the investigation of some processes that could be detected with all-atom molecular dynamics simulation. We show that MD simulation predicts experimental structure of the virus. In addition, it allows us to investigate molecular processes currently undetectable by experiments. In particular, we report the analysis of water and ion flows through the virus capsid and arrive at interesting conclusions that may be important biologically.

Atomistic MD modelling of the whole viral capsid is very resource demanding, it needs to contain all atoms of the system in the calculation, including all water molecules. The fact that the systems usually consist of millions of atoms, where most are water molecules, makes the simulation computationally expensive.

For this reason, we apply our new approach, a hybrid MD/hydrodynamics method that is created with the idea to reduce the simulation cost. The method allows us to represent the system at fully atomistic resolution in the parts where all atoms are necessary, and at much cheaper continuous resolutions in the rest of the system. We have tested our approach on smaller systems [15,16] and now we report its

* Corresponding author.
E-mail address: d.nerukh@aston.ac.uk (D. Nerukh).

http://dx.doi.org/10.1016/j.molliq.2017.06.124
0167-7322/

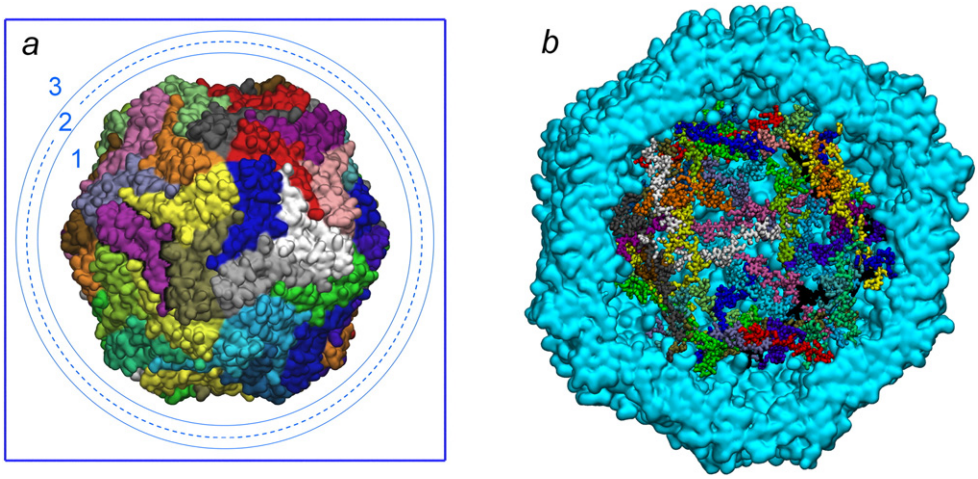

Fig. 1. The initial structure of the capsid: a) the overview with the boundaries of the simulation box and the division of the system onto regions: 1 — pure MD region, 2 — hybrid region, 3 — pure hydrodynamics region; the dashed line shows the subdivision of the hybrid region for thermostating; b) the cross-cut showing the "tails" (system B); the individual proteins (a) or tails (b) are shown in different colour.

application to a virus simulation. The realisation of the hybrid MD/hydrodynamics method for the viral capsid will allow to significantly increase the simulation time. Here we show that our method can successfully simulate the virus preserving its atomistic structure and producing similar dynamical behaviour.

For our study we have chosen the capsid of the porcine circovirus type 2 (PCV2), because PCV2 is the smallest virus with the diameter of about 20 nm and with circular DNA inside [17]. The capsid of PCV2 is stable without the genome and its atomistic structure is defined from X-ray crystallography [1]. However, the N-termini of the capsid have not been detected in the experiment, probably, because of their flexible or disordered structure. The combination of these facts makes this viral capsid a convenient model for all-atom MD simulations.

We have simulated two cases of the whole viral capsid at atomistic resolution: with N-termini (we call them "tails") and without them. Both structures are stable in physiological environments and they have good agreement with experimental data. We have demonstrated in our previous paper [18] the small value of the RMSD for the structures compared to the X-ray structure.

In this report we focus on the detailed analysis of the flow of water molecules and ions in and out the capsid. This is an important process that defines several biological properties of the virus, for example, its mechanical strength under the influence of pressure changes. We show that water exhibits substantial rate of exchange across the capsid's wall, while ions essentially do not permeate the wall. This makes the capsid shell to function as a semipermeable membrane, the behaviour also demonstrated for other viruses [9].

2. Materials and methods

2.1. System preparation

All-atom MD simulation has been performed with explicit model of solvent using GROMACS. For the simulations we used X-ray structure [1] that is deposited in Protein Data Bank (3R0R), and the sequence of N-terminus, which is not detected with X-ray, probably because of their flexible or disordered structure. Therefore, we have reconstructed the structure of the missing N-termini with homology modelling approach in MODELLER [19] and, then, we have assembled the 60 proteins into the whole capsid using Viperdb [20].

We have prepared two initial structures of the capsid: the first one was without the N-termini (Fig.1a) and the second one with the N-termini (Fig.1b), (we will call them "A" and "B" systems respectively).

The capsid is charged highly positively (360 e), while the tails are charged negatively (−3 e per tail). The system is divided by the capsid in two parts: the cavity and the outer solution, which raises the problem of correct neutralization of the system's charge. To solve it we estimated the radial distribution of the capsid's charge by splitting the capsid into a number of concentric spherical layers with the centres located at the capsid centre of mass (COM). The incremental charge of layers was plotted depending on the radius of the largest layer, Fig. 2. It could be seen that the integral capsid charge increases with distance up to ≈7.8 nm and then decreases. This fact indicates that the capsid is highly polarized with the inner surface having a large positive charge, and the negatively charged outer surface. Therefore, to correctly neutralize the capsid we neutralized each surface separately. The number of Cl^- ions equal to the height of the peak on the charge plot, were placed inside the capsid, while to the outer solution, Na^+ ions were added in the amount equal to the difference between the total capsid charge and the charge of the inner surface. These values are listed in Table 1. Finally, additional 1720 Na^+ and Cl^- ions were randomly distributed across the cell, which corresponded to physiological solution concentration (0.9 wt% NaCl). We stress that the total charge of both simulation cells was zero.

Pure MD simulation has been performed using AMBER03 force field with TIP3P water model. The total number of atoms in the system was 1,898,573 for system A and 1,897,998 for system B. The simulated systems had only protein capsid, water, and ions without nucleic acids.

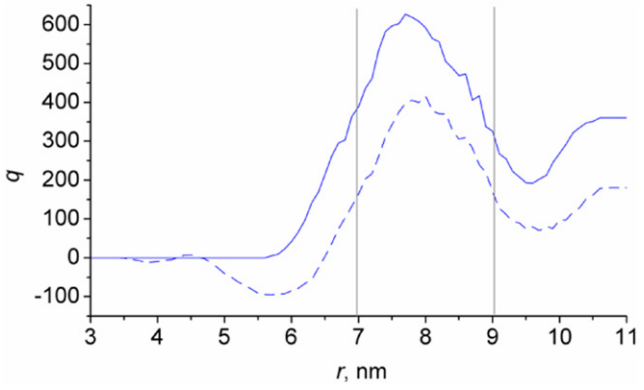

Fig. 2. The dependence of the integral charge of the capsid layers on the radius of the largest layer; the solid curve corresponds to system A, the dashed curve corresponds to system B; vertical lines indicate the approximate boundaries of the capsid wall.

Table 1
The number of ions added to the capsids for charge neutralization.

Capsid	Added ions	
	Inside	Outside
With tails	407 Cl^-	227 Na^+
Without tails	606 Cl^-	246 Na^+

After energy minimization we fixed the capsid with position restraints and a calculation was carried out at $T = 200$ K, following the increase of temperature up to 300 K. After 1 ns of this procedure, the position restrains were switched off and MD simulation of the system was performed at 300 K for 10 ns. The parameters of the simulation were the following: PME treatment of electrostatic forces, 1.0 nm cut-off of van der Waals interactions, velocity-rescale thermostat with time constant of 0.1 ps.

2.2. Calculation of the water and ion flows through the capsid

We used the following algorithm to calculate the number of ions and water molecules located inside the capsid. First, the capsid was divided into 20 × 20 sectors with the vertices in the capsid COM. Then in each sector the distance of each atom to the capsid COM was calculated, and the conventional location of the border between the cavity and the outer solution was determined as an average of atom–capsid COM distances:

$$r_{border} = \frac{1}{N}\sum_{i=1}^{N} r_i$$

This approach makes the value of r_{border} robust to fluctuations in positions of individual atoms. The tail atoms do not form the capsid wall and thus they were not accounted for. Now, an atom was considered to reside inside the capsid if its distance to the capsid COM was less than r_{border}. Using this criterion, in each sector the indices of water molecules and ions located inside the capsid were printed, their counts were calculated, and finally summed together.

To estimate the flows between the cavity and the outer solution we compared the indices of water molecules and ions located inside the capsid between two time moments. The molecules which are inside the capsid in the first (second) time and are not in the second (first) one are considered to have left (entered); and the sum of the left and entered molecules or ions produce the total flow across the capsid wall in the time interval between the first and the second time moments.

2.3. Hybrid methodology

In the current work, following [15,16], we consider a hybrid multiscale model consisting of the continuum hydrodynamics and the molecular dynamics part for the virus simulations.

In the region of interest, i.e. in the volume containing the virus capsid with some water shell atoms around, the hybrid model is used in the pure molecular dynamics mode. Away from that region, the bulk water properties are approximated by continuum fluid dynamics. The coupling is achieved in the so-called acyclic or one-way coupled scheme way [21]. The one-way coupling means there is no feedback from the molecular dynamics particles onto the fluid dynamics part of the model that is described statistically. One can say that within this implementation the fluid dynamics affects the molecular dynamics (MD) as an effective "heat bath" that preserves the correct thermal fluctuations when the hybrid multiscale model is switched to the continuum hydrodynamics regime away from the virus.

For macroscopically stationary liquids in the absence of major hydrodynamic gradients and away from solid boundaries, thermal fluctuations are the only source of macroscopic fluctuations in liquids. These are described by the Landau-Lifshitz Fluctuating Hydrodynamics

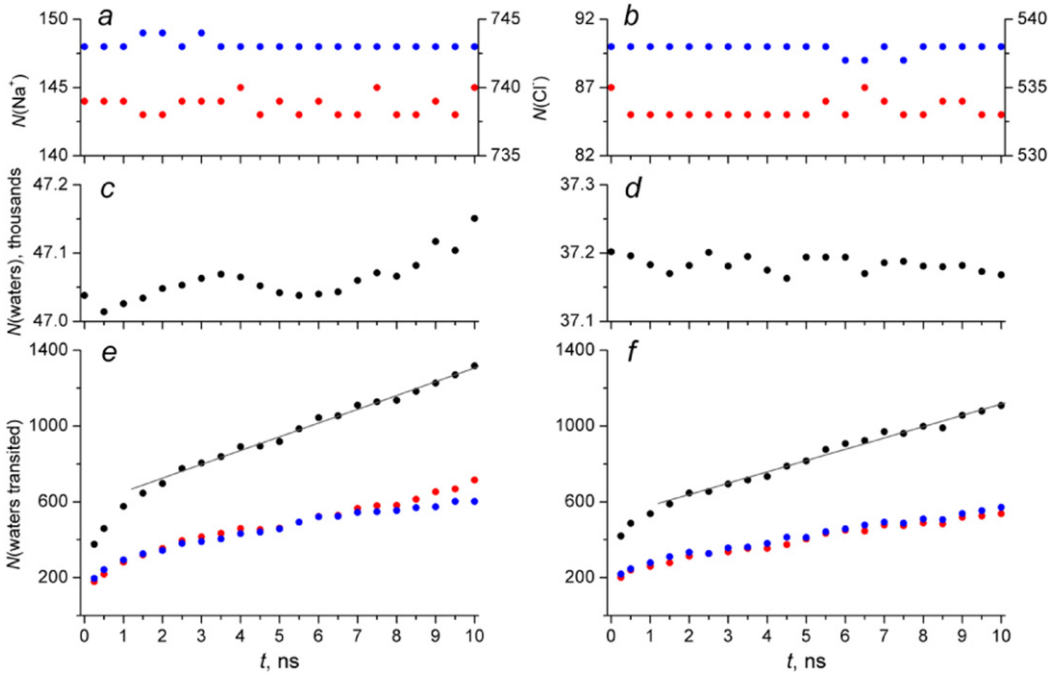

Fig. 3. Water and ions flows in system A (a,c,e) and system B (b,d,f) during 10 ns of simulation; a,b) the number of Na^+ (red) and Cl^- (blue) ions inside the capsid as function of time, c,d) the number of water molecules inside the capsid as function of time, e,f) the total number of water molecules that crossed the capsid wall in both directions compared to the initial structure (black) and its linear fit (grey), the number of entered (red) and left (blue) water molecules.

(LL-FH) equations [22]:

$$\begin{aligned}&\frac{\partial\overline{\rho}}{\partial t}+\ div(\overline{\rho}\cdot\overline{\mathbf{u}})=0,\\&\frac{\partial(\overline{\rho}\cdot\overline{u}_i)}{\partial t}+\ div(\overline{\rho}\cdot\overline{u}_i\cdot\overline{\mathbf{u}})=\sum_{j=1,3}\nabla_j\left(\Pi_{ij}+\tilde{\Pi}_{ij}\right),\ i=1,2,3\end{aligned}\tag{1}$$

where ρ, **u**, p are the density, velocity vector and pressure variables, the bar indicates that the variables are referred to the continuum hydrodynamics. The Equation Of State (EOS), $\overline{p}=\overline{p}(\overline{\rho})$, and the shear and bulk viscosity coefficients, η and ζ, of the Reynolds stress $\mathbf{\Pi}$ and its fluctuating component $\tilde{\mathbf{\Pi}}$,

$$\begin{aligned}&\Pi_{i,j}=-(\overline{p}-\zeta div\overline{\mathbf{u}})\delta_{i,j}+\eta\left(\partial_i\overline{u}_j+\partial_i\overline{u}_j-2D^{-1}\ div\overline{\mathbf{u}}\delta_{i,j}\right),\\&\tilde{\Pi}_{i,j}=\zeta div\tilde{\mathbf{u}}\delta_{i,j}+\eta\left(\partial_i\tilde{u}_j+\partial_i\tilde{u}_j-2D^{-1}\ div\tilde{\mathbf{u}}\delta_{i,j}\right),\quad i,j=1,2,3\end{aligned}\tag{2}$$

are defined in accordance with the MD model, and where the stochastic stress tensor $\tilde{\mathbf{\Pi}}$ is described as a random Gaussian matrix with zero mean and covariance, given by the formula

$$\begin{aligned}&\left\langle\tilde{\Pi}_{i,j}(\mathbf{r}_1,t_1)\tilde{\Pi}_{k,l}(\mathbf{r}_2,t_2)\right\rangle\\&\quad=2k_BT\left[\eta\left(\delta_{i,k}\delta_{j,l}+\delta_{i,l}\delta_{j,k}\right)+\left(\zeta-2D^{-1}\eta\right)\delta_{i,j}\delta_{k,l}\right]\delta(t_1-t_2)\delta(\mathbf{r}_1-\mathbf{r}_2).\end{aligned}\tag{3}$$

The LL-FH equations are solved with a central finite-volume method [23] to provide the 'target' cell-centre hydrodynamic variables for the modified MD particle velocity and acceleration, $\frac{d\mathbf{x}_p}{dt}$ and $\frac{du_{ip}}{dt}$, equations:

$$\begin{aligned}&\frac{d\mathbf{x}_p}{dt}=\mathbf{u}_p+s(\overline{\mathbf{u}}-\mathbf{u}_p)+s(1-s)\cdot\alpha\cdot\frac{\sum_{\gamma=1,6}\left(\overline{\rho}-\sum_{q=1,N(t)}\rho_q\right)d\mathbf{n}^\gamma}{\sum_{q=1,N(t)}m_q},\\&\frac{du_{ip}}{dt}=(1-s)F_{ip}/m_{ip}+\\&+\sum_{k=1,3}\sum_{\gamma=1,6}\left(s(1-s)\cdot\alpha\cdot\sum_{q=1,N(t)}\rho_q u_{iq}\cdot\left\langle\frac{\sum_{\lambda=1,6}\left(\overline{\rho}-\sum_{q=1,N(t)}\rho_q\right)dn_k^\lambda}{\sum_{q=1,N(t)}m_q}\right\rangle_\gamma\right)dn_k^\gamma/\sum_{q=1,N(t)}m_q\\&+\sum_{k=1,3}\sum_{\gamma=1,6}\left(s(1-s)\cdot\beta\cdot\frac{1}{V}\left\langle\sum_{\lambda=1,6}\left(\overline{\rho}\cdot\overline{u}_i-\sum_{q=1,N(t)}\rho_q u_{iq}\right)dn_k^\lambda\right\rangle_\gamma\right)dn_k^\gamma/\sum_{q=1,N(t)}m_q,\quad i=1,3,\end{aligned}\tag{4}$$

where $\alpha,\beta>0$ are numerical adjustable constant parameters, which characterize the 'diffusion rate' of the difference between the continuum and the atomistic parts of the model. The latter parameters define how fast the two parts of the same hybrid model equilibrate to the same macroscopic condition, i.e. converge to the same liquid they represent. The characteristic relaxation time associated with these parameters

$$\tau^{diff}\sim\Delta x^2/\alpha\sim\Delta x^2/\beta\tag{5}$$

where $\Delta x=\sqrt[3]{V}$ is the length scale associated with the control volume V, should be comparable to the time step of the particles $\tau^{diff}\sim\tau^{MD}$ so that the relaxation process affects the particle trajectories over their characteristic molecular dynamics time scale.

$s=s(x,y,z)$ is a user-defined domain-decomposition function which specifies how smoothly the hydrodynamic and the atomistic parts of the simulation are distributed across the solution domain. Following the previous work [16], a spherical function is defined so that

$$s(x,y,z)=\begin{cases}S_{\min}, & r\le R_{MD};\\ \dfrac{r-R_{MD}}{R_{FH}-R_{MD}}(S_{\max}-S_{\min})+S_{\min}, & R_{MD}<r<R_{FH};\\ S_{\max}, & r\ge R_{FH}.\end{cases}\tag{6}$$

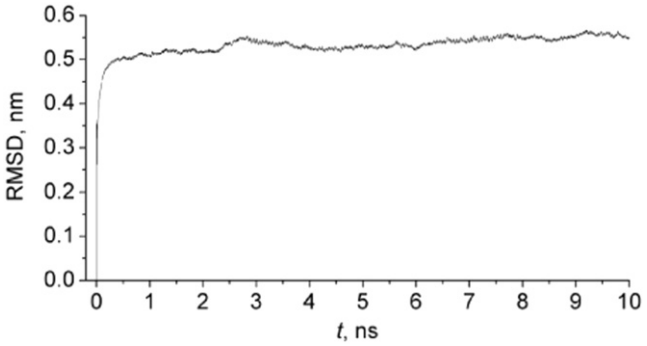

Fig. 4. Root mean square displacement of capsid backbone atoms from the initial configuration during hybrid MD/hydrodynamics run.

where $r=(x-L/2)^2+(y-L/2)^2+(z-L/2)^2$, L is the computation box size, $x,y,z\in[0,L]$, $S_{\min}=0$, $S_{\max}=1$. The function is locked to the centre of mass of the virus capsid ($r=0$), hence, making sure that the virus always remains within the fully atomistic part of the hybrid multiscale model ($s=0$). In this simulation, R_{MD} and R_{FH} equals to 0.85 and 0.95 respectively in order to include the whole capsid and the nearest water in the pure MD region (Fig. 1a).

Detailed derivation of Eq. (4) can be found in [21,16] but the following should be highlighted.

1. The cell-average fields $\overline{\rho}$, $\overline{\mathbf{u}}$, $\sum_{q=1,N(t)}\rho_q$ and $\sum_{p=1,N(t)}\rho_q\mathbf{u}_q$, which appear on the right-hand-side of the above equations, correspond to the centres of the cell-volumes and need to be evaluated for each location $\boldsymbol{x}$ of MD particle p, for example, using a trilinear interpolation in space for the particle location between the cell centre points, and an interpolation in time in case the hydrodynamics solution is advanced in time with a bigger time step in comparison with the MD solution.
2. The summations on the right-hand side correspond to the volume average field gradients (first derivatives and second derivatives in $\frac{d\mathbf{x}_p}{dt}$ and $\frac{du_{ip}}{dt}$ equations, respectively), e.g. using the divergence theorem to eliminate one derivative and assuming the implementation within a finite-volume framework.

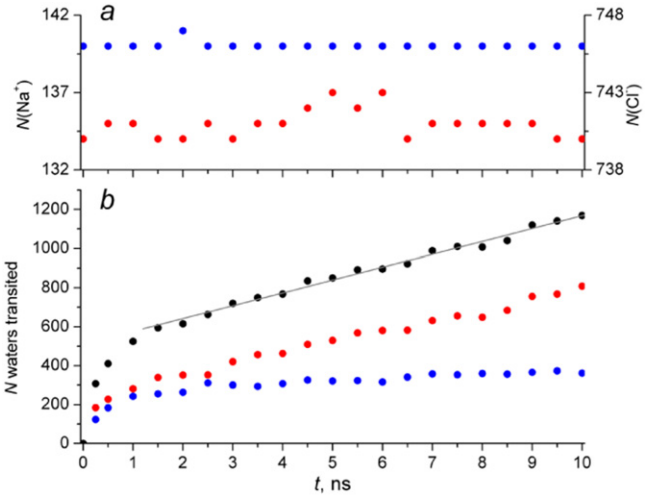

Fig. 5. a) the number of Na^+ (red) and Cl^- (blue) ions inside the capsid as function of time; b) the total number of water molecules that crossed the capsid wall in both directions compared to the initial structure (black) and its linear fit (grey), the number of entered (red) and left (blue) water molecules during the hybrid MD/hydrodynamics run.

3. For the pure hydrodynamics region ($s = 1$), in accordance with the equations above, the particles become passive tracers transported in the hydrodynamics field in accordance with the external boundary conditions imposed by hydrodynamics (periodic boundaries in this case). Thus, there is no need to compute the molecular dynamics potentials in this large area, and the most expensive part of the MD simulation can be avoided.

Special attention should be given to the thermostating of the system. Considering the widely used velocity rescaling thermostats in the standard implementation, the instantaneous temperature is calculated using the velocities of a specified group of atoms (usually the whole system). Then the velocities of these atoms are uniformly rescaled according to the ratio between the instantaneous and the reference temperatures. However, in our hybrid simulations the system is divided into substantially different regions from the thermostating point of view. The temperature of the pure hydrodynamics region is determined by the FH field only, thus, the atoms located in this region at a given time moment should not be accounted for when computing the instantaneous temperature for the thermostat, that is they should not be thermostated. On the contrary, the atoms in the hybrid zone are controlled by the FH field only partially, thus, they should have their velocities rescaled. Therefore, we implemented separate thermostating for the pure MD region, and the two halves of the hybrid region ($s \le 0.5$ and $s > 0.5$, Fig. 1a); the pure hydrodynamics region is left unaffected by thermostating. For each zone the instantaneous temperature and the velocity rescaling were calculated individually.

3. Results and discussion

Both classical MD and hybrid methods produced a stable capsid with small RMSD with respect to the crystal structure. This signifies that the experimentally measured atomistic structure at low temperature and non-physiological conditions is preserved in room temperature solution with cell-like salt background.

We calculated the transport of sodium ions, chloride ions, and water molecules across the capsid wall during 10 ns. Fig. 3a,c,e show the results for system A and Fig. 3b,d,f - for system B. It is important to note that the ranges of the Y axes on corresponding plots are equal to facilitate comparison.

Fig. 3a,b demonstrates the changes of the dynamics of chloride (blue points) and sodium (red points) ions for systems A and B. The number of sodium ions and chloride ions are almost constant during all 10 ns. We note that the number of ions transiting through the capsid wall is negligible and there are no mutually compensating flows of ions in and out of the capsid.

More interesting results are observed for water molecules flow. Fig. 3c,d demonstrates the dependence of the number of water molecules inside the capsid on time. This number fluctuates around a constant value. The fluctuations are of larger period in system A (no tails), Fig. 3c, than in system B (with tails), Fig. 3d. Nevertheless, the water molecules flow is detectable during the simulated 10 ns.

Fig. 3e,f shows the total number of water molecules that crossed the capsid between the initial configuration and the configuration at time t. It is computed as a sum of (i) the number of molecules, which stay inside the capsid in the initial configuration and are outside of it at time t, and (ii) vice versa. The average flow, obtained as a slope of linear fitting of the plots, is 73 ± 3 molecules per ns for system A and 60 ± 2 for system B. Two first ns were not used for fitting because of residual equilibration taking place after the constraints were removed from the capsid atoms.

The capsid structure simulated using our hybrid method shows small RMSD compared to the crystal structure, Fig. 4. This demonstrates that our methodology preserves the atomistic structural properties in the atomistic zone of the system.

The flow of ions is also absent in the hybrid case, in agreement with the pure MD runs (Fig. 5a). In contrast, the flow of water amounts to 66 ± 2 molecules per ns, which is somewhat (by 10%) lower than in the pure MD simulation, Fig. 5b. This shows that the hydrodynamics part of the simulation still distorts the dynamics of the atomistic motion, but the effect is of limited magnitude. A noticeable effect is the large difference between the magnitudes of ingoing and outgoing flows. We are currently investigating the reasons of these deviations.

4. Conclusions

We performed the analysis of water molecules and ions flows across the viral capsid wall. The analysis has been done for the viral capsid structures obtained from the X-ray and simulated using all-atom molecular dynamics with explicit solvent model for 10 ns. The analysis demonstrates that during 10 ns the ions from the solution essentially do not cross the capsid shell. This is in contrast to water molecules that possess the ability of transiting across the capsid wall in both directions. All-atom MD simulation of poliovirus in [9] exhibits similar behaviour of molecular permeability of the poliovirus capsid. The authors concluded that the poliovirus capsid can work as semipermeable membrane. We here observe similar behaviour. This function of the capsid can play an important mechanical role in withstanding high pressures or pressure changes. The simulation of the same system in the hybrid MD/hydrodynamics approach produced the virus structure and the magnitudes of ions and water flows close to those obtained in pure MD simulation, which validates our approach.

Acknowledgements

E.T. acknowledges support from the Royal Society of Chemistry (Researcher Mobility Fellowship, 550074), the Great Britain Sasakawa Foundation (grant 4679), and the 5 top 100 Russian Academic Excellence Project at the Immanuel Kant Baltic Federal University (5-100).

This work used the ARCHER UK National Supercomputing Service (http://www.archer.ac.uk) funded by the UK High-End Computing Consortium for Biomolecular Simulation (grant number EP/L000253/1), the RIKEN Integrated Cluster of Clusters (RICC) and HOKUSAI GreatWave system. I.K. gratefully acknowledges the financial support of European Commission under the Marie Curie Individual Fellowship (H2020-MSCA-IF-2015-700276 “HIPPOGRIFFE” project).

The supporting data of this study are stored at the University of Aston. Details of how to request access to these data are provided in the documentation available from the University of Aston research data repository at http://doi.org/10.17036/researchdata.aston.ac.uk.00000213

References

[1] R. Khayat, N. Brunn, J.A. Speir, J.M. Hardham, R.G. Ankenbauer, A. Schneemann, J.E. Johnson, The 2.3-angstrom structure of *Porcine circovirus* 2, J. Virol. 85 (2011) 7856–7862.
[2] S.W. Lane, C.A. Dennis, C.L. Lane, C.H. Trinh, P.J. Rizkallah, P.G. Stockley, S.E. Phillips, Construction and crystal structure of recombinant STNV capsids, J. Mol. Biol. 413 (2011) 41–50.
[3] S. Duquerroy, B. Da Costa, C. Henry, A. Vigouroux, S. Libersou, J. Lepault, J. Navaza, B. Delmas, F.A. Rey, The Picobirnavirus crystal structure provides functional insights into virion assembly and cell entry, EMBO J. 28 (2009) 1655–1665.
[4] X. Wang, J. Ren, Q. Gao, Z. Hu, Y. Sun, X. Li, D.J. Rowlands, W. Yin, J. Wang, D.I. Stuart, Z. Rao, E.E. Fry, Hepatitis A virus and the origins of Picornaviruses, Nature 517 (2015) 85–88.
[5] G. Zhao, J.R. Perilla, E.L. Yufenyuy, X. Meng, B. Chen, J. Ning, J. Ahn, A.M. Gronenborn, K. Schulten, C. Aiken, P. Zhang, Mature HIV-1 capsid structure by cryo-electron microscopy and all-atom molecular dynamics, Nature 497 (2013) 643–646.
[6] D.S. Larsson, L. Liljas, D. van der Spoel, Virus capsid dissolution studied by microsecond MD simulation, PLoS Comput. Biol. 8 (2012), e1002502.
[7] J.R. Perilla, J.A. Hadden, B.C. Goh, C.G. Mayne, K. Schulten, All-atom molecular dynamics of virus capsids as drug targets, J. Phys. Chem. Lett. 7 (2016) 1836–1844.
[8] P.L. Freddolino, A.S. Arkhipov, S.B. Larson, A. McPherson, K. Schulten, Molecular dynamics simulations of the complete satellite tobacco mosaic virus, Structure 14 (2006) 437–449.

[9] Y. Andoh, N. Yoshii, A. Yamada, K. Fujimoto, H. Kojima, K. Mizutani, A. Nakagawa, A. Nomoto, S. Okazaki, All-atom molecular dynamics calculation study of entire poliovirus empty capsids in solution, J. Chem. Phys. 141 (2014) 165101.
[10] Y. Miao, J.E. Johnson, P.J. Ortoleva, All-atom multiscale simulation of cowpea chlorotic mottle virus capsid swelling, J. Phys. Chem. B 114 (2010) 11181–11195.
[11] M. Zink, H. Grubmüller, Primary changes of the mechanical properties of southern bean mosaic virus upon calcium removal, Biophys. J. 98 (2010) 687–695.
[12] J.R. Perilla, B.C. Goh, C.K. Cassidy, B. Liu, R.C. Bernardi, T. Rudack, H. Yu, Z. Wu, K. Schulten, Molecular dynamics simulations of large macromolecular complexes, Curr. Opin. Struct. Biol. 31 (2015) 64–74.
[13] I. Ohmura, G. Morimoto, Y. Ohno, A. Hasegawa, M. Taiji, MDGRAPE-4: a special-purpose computer system for molecular dynamics simulations, Philos. Transact. A Math. Phys. Eng. Sci. 372 (2014) 20130387.
[14] D.E. Shaw, J.P. Grossman, J.A. Bank, B. Batson, J.A. Butts, J.C. Chao, M.M. Deneroff, R.O. Dror, A. Even, C.H. Fenton, et al., Anton 2: Raising the bar for performance and programmability in a special-purpose molecular dynamics supercomputer, Proceedings of the International Conference for High Performance Computing, Networking, Storage and Analysis (SC14), IEEE, Piscataway, NJ 2014, pp. 41–53.
[15] I. Korotkin, S. Karabasov, D. Nerukh, A. Markesteijn, A. Scukins, V. Farafonov, E. Pavlov, A hybrid molecular dynamics/fluctuating hydrodynamics method for modelling liquids at multiple scales in space and time, J. Chem. Phys. 143 (2015), 014110.
[16] I. Korotkin, D. Nerukh, E. Tarasova, V. Farafonov, S. Karabasov, Two-phase flow analogy as an effective boundary condition for modelling liquids at atomistic resolution, J. Comput. Sci. 17 (2016) 446–456.
[17] B. Yang, H. Wang, C. Ho, P. Lester, Q. Chen, F. Neske, S.A. Baylis, J. Blumel, Porcine circovirus (PCV) removal by Q sepharose fast flow chromatography, Biotechnol. Prog. 29 (2013) 1464–1471.
[18] E. Tarasova, V. Farafonov, R. Khayat, N. Okimoto, T.S. Komatsu, M. Taiji, D. Nerukh, All-atom molecular dynamics simulations of entire virus capsid reveal the role of ion distribution in Capsid's stability, J. Phys. Chem. Lett. 8 (2017) 779–784.
[19] A. Sali, T.L. Blündell, Comparative protein modelling by satisfaction of spatial restraints, J. Mol. Biol. 234 (1993) 779–815.
[20] M. Carrillo-Tripp, C.M. Shepherd, I.A. Borelli, S. Venkataraman, G. Lander, P. Natarajan, J.E. Johnson, C.L. Brooks, V.S. Reddy, VIPERdb2: an enhanced and web API enabled relational database for structural virology, Nucleic Acids Res. 37 (2009) D436–D442.
[21] S. Karabasov, D. Nerukh, A. Hoekstra, C. Chopard, P.V. Coveney, Multiscale modelling: approaches and challenges, Philos. Trans. R. Soc. A Math. Phys. Eng. Sci. 372 (2014), 20130390.
[22] L.D. Landau, E.M. Lifshitz, Statistical Physics, Part 1, Elsevier, Amsterdam, 1980.
[23] A.P. Markesteijn, S.A. Karabasov, V.Y. Glotov, V.M. Goloviznin, Comput. Methods Appl. Mech. Eng. 281 (2014) 29–53.